To be published in Applied Optics:

Title: Modeling UV-C Irradiation Chambers for Mask Decontamination using Zemax OpticStudio

Authors: Thomas Baer,Lambertus Hesselink,Jeff Wilde

Accepted: 19 July 20

Posted 21 July 20

DOI: https://doi.org/10.1364/AO.402603

Modeling UV-C Irradiation Chambers for Mask Decontamination using Zemax OpticStudio

Jeffrey P. Wilde[1,2*], Thomas M. Baer[1,2], and Lambertus Hesselink[1,2,3]
[1]*E. L. Ginzton Laboratory, Stanford University, Stanford, CA 94305*
[2]*Stanford Photonics Research Center, Stanford University, Stanford, CA 94305*
[3]*Department of Electrical Engineering, Stanford University, Stanford, CA 94305*
**Corresponding author:* jpwilde@stanford.edu

Abstract

Ultraviolet decontamination of personal protective equipment, particularly masks, is important in situations where mask reuse is practiced. To assist in the development of UV-C decontamination chambers, we have constructed ray tracing models in Zemax OpticStudio v20.1 for two distinct geometries, namely a rectangular cabinet and a cylindrical can. These models provide irradiance distributions that can be used for comparison with experiment and as well as to predict local irradiance variation over the surface of a mask. In this paper we describe the model details, including: (1) a mask object in CAD format, (2) our assumptions for modeling surface properties, (3) the use of polygon object detectors for local irradiance analysis, and (4) experimental results that compare favorably to the simulations.

1. Introduction: UV-C Illumination for Pathogen Decontamination

With the onset of the COVID-19 pandemic, there has been renewed interest in using UV radiation for decontamination of filtering facepiece respirators (FFRs), in particular, N95 masks. For this purpose, UV-C radiation, ranging in wavelength from 200 nm to 280 nm (also referred to as UV Germicidal Irradiation, or UVGI), is deemed the most effective form of UV because light in this wavelength regime is strongly absorbed by nucleic acids [1]. The N95DECON organization, a volunteer consortium of scientists and technical experts, has issued a report [2] regarding UV-C decontamination of N95 masks in which they state, "We find in the literature that a UV-C irradiation dose of ≥ 1.0 J/cm^2 at the FFR surface inactivates SARS-CoV-2 analogues (≥3-log reduction) on the majority of tested N95 facepieces." While work continues in this area, the CDC [3] recommends that "Decontamination and subsequent reuse of FFRs should only be practiced where FFR shortages exist."

Commercial UV mask decontamination units are available [4, 5], and various medical groups have devised room-scale techniques for processing a large number of masks at one time [6, 7]. We recently joined a collaborative group with a primary goal of producing public-domain, do-it-yourself (DIY) designs for UV-C mask decontamination systems that can be constructed using readily available, low-cost components [8]. Two design configurations have been explored: (1) a metal office cabinet, and (2) a small metal trash can. For this work, optical ray-trace modeling using Zemax OpticStudio v20.1 proves helpful during the design and prototype evaluation phases. We find that the simulation results bear a reasonably close resemblance to the directly measured irradiance levels. The model implementation details are reported here.

2. Non-Sequential Models of Irradiation Chambers: Component Details

2.1 Modeling Objectives

When designing an illumination chamber for mask decontamination, the irradiance distribution over a mask surface is of key importance. Ideally the illumination should be fairly uniform and of sufficient

strength to reach the 1 J/cm^2 exposure target in a reasonable time. For example, with an irradiance of 10 mW/cm^2, this level of exposure occurs in 100 seconds. The goals of the model are to therefore: (1) provide irradiance distributions as "seen" by a mask across its surface, as well as to (2) mimic test measurements made in actual prototype units.

2.2 UV-C Lamps

A low-pressure mercury-vapor lamp has a strong emission line at 254 nm. Lamps of various sizes and powers are available. We use the Biolux lamp fixtures from Atlantic Ultraviolet Corporation [9] as shown in Fig. 1. In OpticStudio, a lamp bulb can be modeled by a monochromatic, randomly polarized "Source Tube" assigned a system wavelength of 0.254 um. The lamp fixture base (containing an internal ballast) is polished chrome, and can be modeled as either a "Rectangular Volume" or an "Extruded" object (if the 45-degree beveled edge detail is desired).

Model:		25 Watt	30 Watt
Volts: ①		120v	120v
Hertz:		60Hz	60Hz
Amps:		0.25	0.33
Lamp	Lamp:	05-1107-R	05-1106-R
	Power Consumption: ②	25.0w	30.5w
	Ultraviolet Output: ③	6.9w	11.6w
	Ave. Effective Life: (Hrs)	8,000	8,000
Length: (in)		19-1/2	37-1/2
Width: (in)		2-5/8	2-5/8
Height: (in)		3-1/2	3-1/2

Fig. 1. Biolux germicidal UV-C (λ = 254 nm) lamp fixture specifications.

2.3 Mask Model

In OpticStudio, we use a CAD version of an N95 mask as shown in Fig. 2.

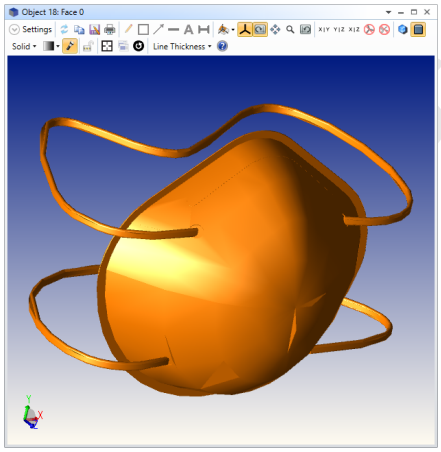

Fig. 2. CAD model of an N95 mask (STEP file format).

Transmission and reflection properties can be specified by means of a custom coating. Surface scattering from the fabric can be added to mimic the diffuse transmission and reflection. More detail is deferred to Section 2.5.

2.4 Two Enclosure Configurations

Two basic system configurations have been explored: (1) a rectangular metal cabinet, and (2) a cylindrical metal trash can. One specific cabinet design is shown below in Fig. 3. It is based on a standard metal office cabinet having dimensions 72" (H) x 36" (W) x 24" (D). The interior is lined with aluminum foil, and 16 lamps (11.6 watts each) are mounted inside, with 8 on the back wall and 8 on the front doors. Up to forty masks (8 rows, 5 masks/row) can be pre-arranged on a rack and then loaded into the cabinet.

Fig. 3. Cabinet decontamination configuration. A CAD model with 28 masks is shown on the top, and a photograph of an empty prototype unit is on the bottom.

The cylindrical trash can configuration is shown in Fig. 4. Its circular symmetry provides very uniform illumination. This unit has a 20-inch diameter and is 27 inches tall. It is also lined inside with aluminum foil, and then eight lamps (6.9 watts each) are mounted to the interior wall. A simple mask support frame made out of PVC tubing, wrapped with aluminum foil, allows 3-4 masks to be illuminated at a time. This frame can also be pre-loaded with masks and very quickly swapped out with one inside the

unit, so the effective loading time is quite short (< 30 seconds). Once the masks are loaded, the lid is placed on top and the illumination started.

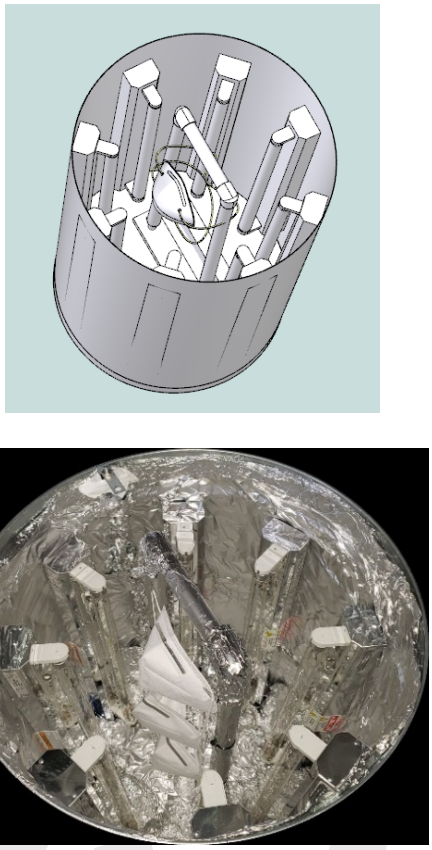

Fig. 4. Cylindrical trash can decontamination configuration. A CAD model is shown on the top, and a photograph of a prototype unit is on the bottom.

2.5 Object Surface Properties & Non-Sequential Ray Settings

Proper modeling of the illumination chambers requires a thoughtful choice for the reflectivity, transmission, and scattering characteristics of the various surfaces involved. In our case we only have three distinct surfaces: (1) aluminum foil lined enclosure walls, (2) polished chrome lamp fixture surfaces, and (3) mask surfaces. The surface property values we selected are summarized in Table 1.

			Scattering		
Surface	Intensity Reflection (R)	Intensity Transmission (T)	Type	Scatter Fraction	Specular Fraction
Al Foil (matte side)	73%	0%	Lambertian	70%	30%
Polished Chrome	80%	0%	None	N/A	100%
Mask	5%	1%	Lambertian	100%	0%

Table 1. Summary of the assumed surface properties as modeled in OpticStudio.

The aluminum foil is typically crinkled after installation. Also, we use the matte side (as opposed to the shiny side) for a more diffuse reflection -- so we do not treat the foil like a smooth specular reflecting surface, but instead use 70% Lambertian scattering as a convenient, albeit speculative, approximation.

The reflectivity and transmission can be easily implemented with an "IDEAL" coating by adding the following lines to the COATING.DAT file (and renaming the file so it is not overwritten by a subsequent OpticStudio version update):

```
! IDEAL <name> T R TIR
IDEAL R.73_T.00  0.00  0.73
IDEAL R.80_T.00  0.00  0.80
IDEAL R.05_T.01  0.01  0.05
```

The scattering properties are specified in the "Coat/Scatter" portion of an object's properties tab. Figure 5 shows an example for the cabinet walls.

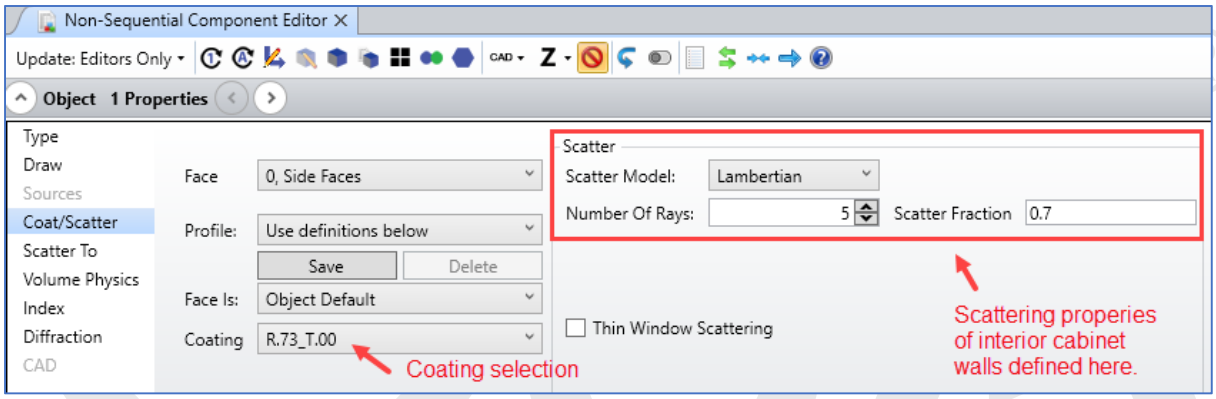

Fig. 5. Specification of cabinet interior wall coating and scattering properties.

For Lambertian scattering, we specify that five scattered rays be randomly generated for each incident ray. Note that the only object with a non-zero surface transmission is a mask, so in general with scattering turned on, a ray incident on a mask will split into reflected and transmitted ray groups. However, to help reduce the computational load, we opt to use the "Simple Ray Splitting" feature that forces either the reflected ray segment group or the transmitted ray segment group to be generated, but not both. The choice is random for each incident ray, with the relative probabilities determined by the values of R and T. To properly account for the surface properties, and to ignore occasional (but typically very rare) ray trace errors, simulations should be executed with the options indicated on the left of Fig. 6.

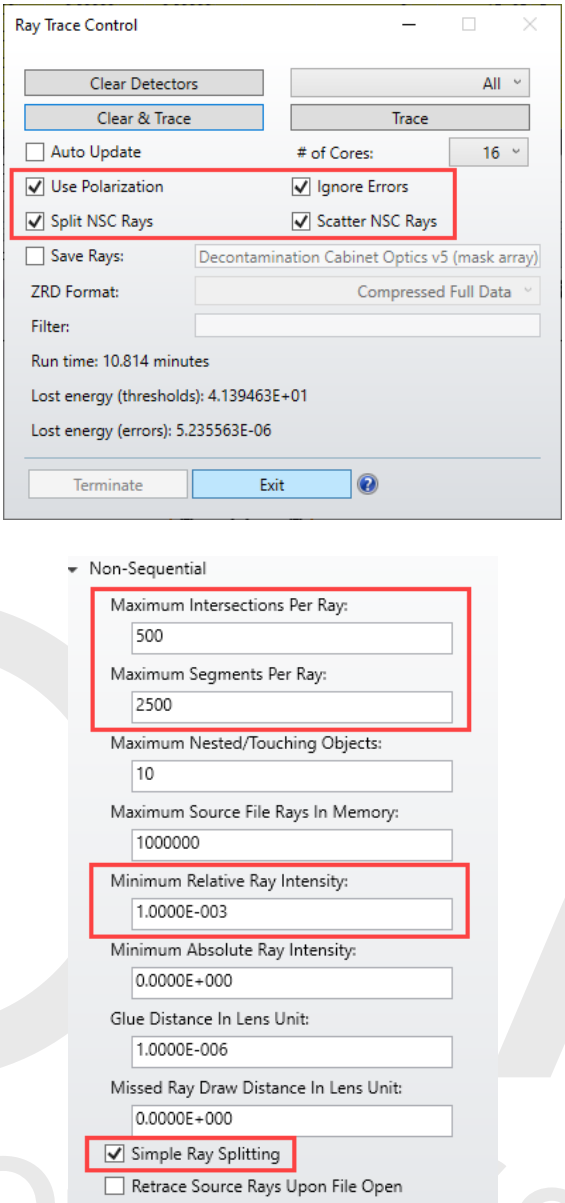

Fig. 6. Left: Non-sequential ray trace control settings. Right: Parameter values that affect the number of ray segments created during a simulation run.

Also, as shown in Fig. 6, we restrict the maximum intersections per ray to 500, the maximum segments per ray to 2500, and the minimum relative ray intensity to 0.001. In practice, the minimum relative ray intensity will typically limit the number of ray segments. For example, assume there are n_R reflections from a given surface, with each reflected ray segment subsequently scattering (i.e., splitting) into n_S new segments. It's simple to show that the total number of segments associated with one source ray is

$$N_{seg} = \sum_{i=0}^{n_R} (n_S)^i, \tag{1}$$

and the average relative intensity per segment (following the last reflection) becomes

$$I_{avg} = \left(\frac{R}{n_S} \right)^{n_R}, \qquad (2)$$

where R is the surface reflectivity. Again, let's assume n_S = 5 (as shown in Fig. 5). After only four reflections from the aluminum foil (R = 0.73), we have N_{seg} = 781 and I_{avg} = 5 x 10^{-4}. Therefore, with the minimum relative ray intensity set to 1 x 10^{-3}, we can reasonably expect that any given source ray will split into no more than about 500-700 ray segments, well below the limit of 2,500 as set in Fig. 6.

3. Non-Sequential Models of Irradiation Chambers: System Examples

We now describe our OpticStudio models created for simulation of both the cabinet and cylindrical trash can irradiation geometries. For both models we use a single system wavelength of 0.254 um.

3.1 Cabinet Geometry (up to 40 masks)

The cabinet has 16 lamps (11.6 watts of UV each). The mechanical design comprises groups of lamps that are staggered with respect to one another. To mimic this layout, we use the Source Tube (L = 35", D = 1") object to represent a lamp, and take advantage of the source array capability to first place a group of four lamps in the upper part of the back wall (see Fig. 7).

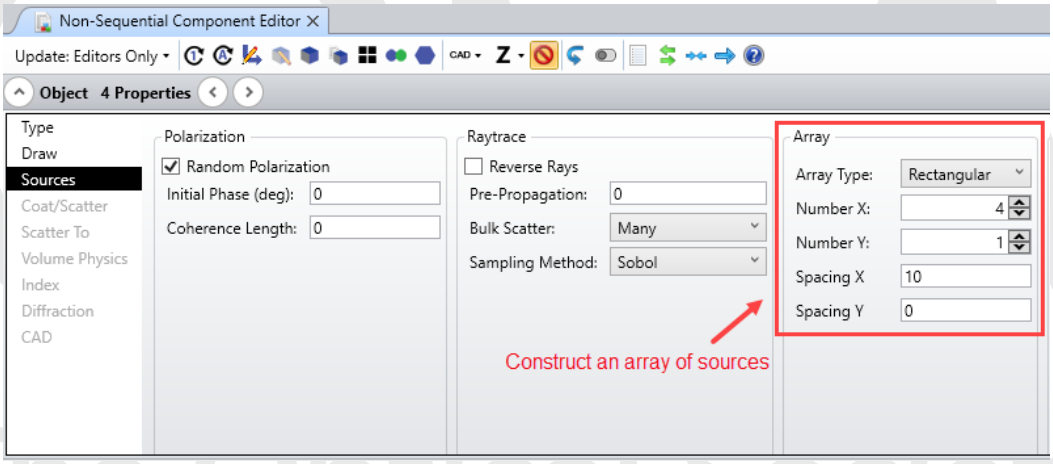

Fig. 7. Method for constructing an array of source lamps.

We then do the same for the lower region of the back wall. On the interior of the front doors, we use four groups of lamps, with each group containing a two-element array. Overall, a simpler design for placing the cabinet lamps could use just two arrays, one for the back wall and a second array for the front, but in this case each array would have to be strictly rectangular with uniform spacings and no offsets. Each lamp has a polished chrome fixture, approximated by a rectangular block. The fixtures are arrayed in precisely the same way as the lamps are, but in this case there is one parent fixture, and we use a single "Array" object to tile the fixtures.

To measure the irradiance levels, we place a Detector Rectangular object in the center of the cabinet with a size sufficient to span the cross-sectional area of the cabinet. The detector is transparent, so as not to alter the rays, and it is set for one-sided detection (either back-facing or door-facing). This detector scheme yields results that can be compared to the physical measurements we made by placing

a small detector on a rod and translating it horizontally and vertically (through small holes cut on the side and top of the cabinet). A 3D Layout of the cabinet, fully populated with lamps and the detector surface, is shown in Fig. 8. The detector yields a 2D irradiance map as shown in Fig. 9, with horizontal and vertical cross sections that also show experimental measurement points. It is seen that the OpticStudio model does a nice job of matching the measurements. The simulation uses 10^5 rays/lamp, for a total of 1.6 million source rays. Approximately 66.5 million ray segments end up being detected. On a dual-CPU (Intel Xeon E5520 2.27 GHz processors), 8-core hyperthreaded workstation, the simulation runtime is 10.8 minutes when using all available 16 threads.

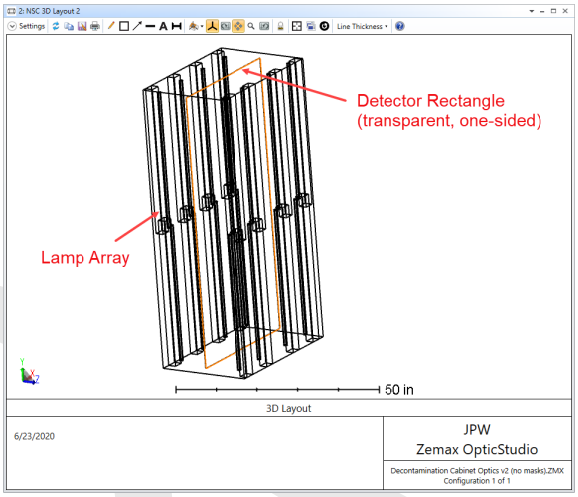

Fig. 8. Layout of the cabinet model without masks installed.

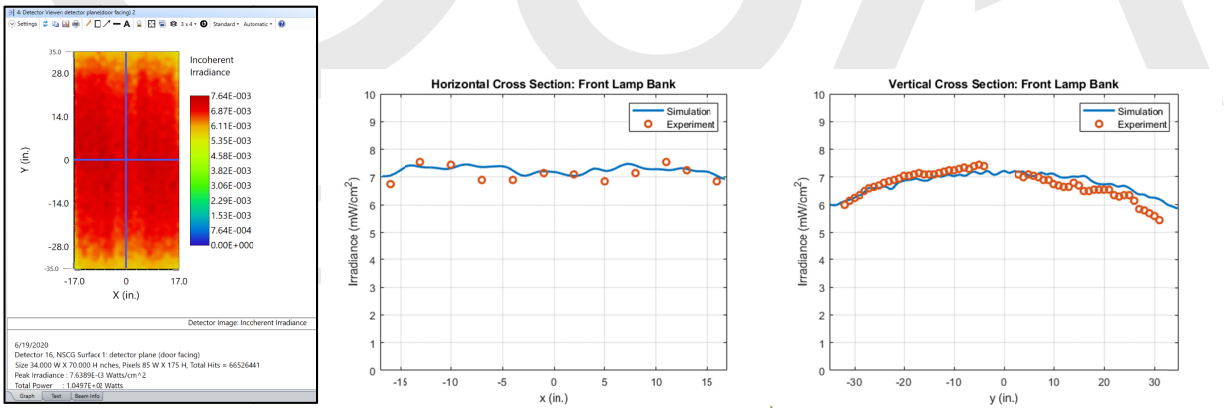

Fig. 9. Top: Simulated door-facing 2-D irradiance map measured in the center of the cabinet (no masks, 10^5 rays/lamp). Bottom: horizontal and vertical cross sections which include experimental data points.

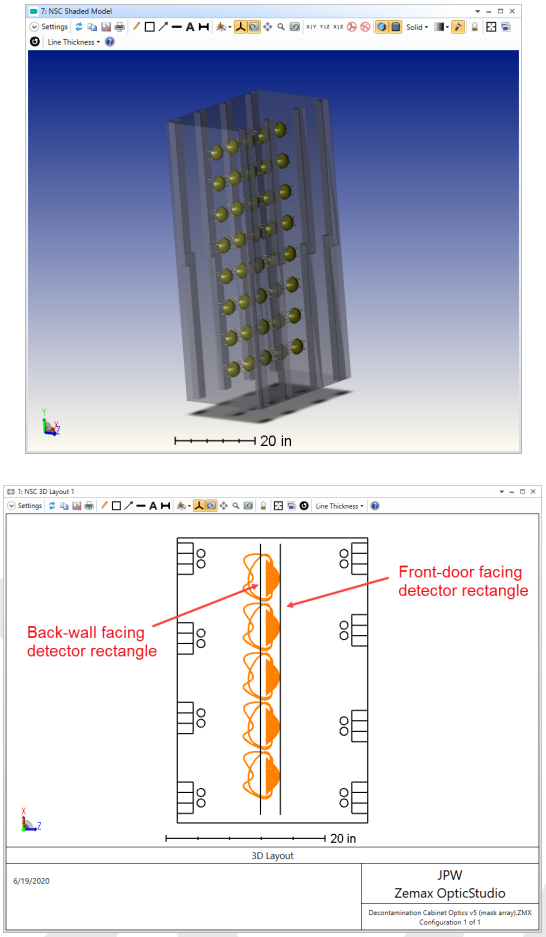

Fig. 10. An array of 40 masks are added to the model.

An array of masks can be added using the CAD version of a mask described in Section 2.3 (with surface properties as indicated in Table 1). Figure 10 shows a shaded perspective view on the left, and a top view of the layout on the right. A second Detector Rectangle object is included so that there is now a detector on either side of the mask array, with one detector facing the back wall and the other facing the front doors. In this case the simulation runtime is 21 minutes. The irradiance level with the masks installed drops by about 15%, to around 6 mW/cm^2, compared to the no-mask situation.

Of particular interest is the variation of local irradiance over the surface of a mask. One possible approach to finding this distribution is to convert a mask into a detector, with the tessellation triangles that represent the surface serving as pixels. However, the native tessellation of a CAD object can yield a wide range of triangle shapes and sizes, including very small triangles that do not receive enough rays to make meaningful estimates of the irradiance for the corresponding pixels. Instead, a better approach is to use a polygon object as a detector because it can be constructed with equal-area triangles. For example, Fig. 11 shows how to use the "Create Polygon Object" tool in the non-sequential editor (NSE) to make a sphere having 512 triangular pixels, all with the same shape and size.

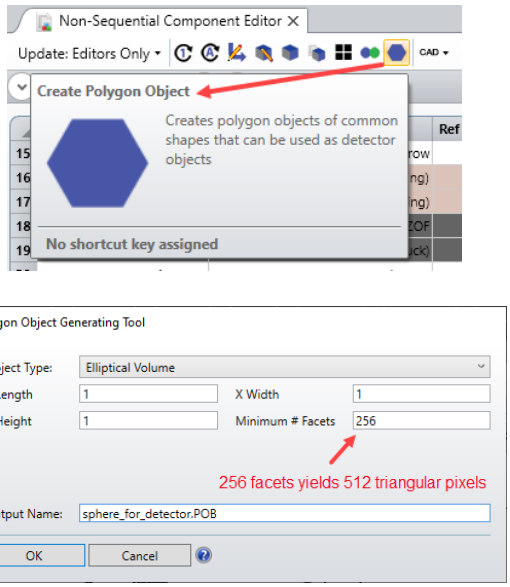

Fig. 11. Use the "Create Polygon Object" tool and select the "Elliptical Volume" option to make a unit sphere with 256 facets (512 triangular pixels) written as a *.POB file in the \ZEMAX\Objects\Polygon Objects directory folder.

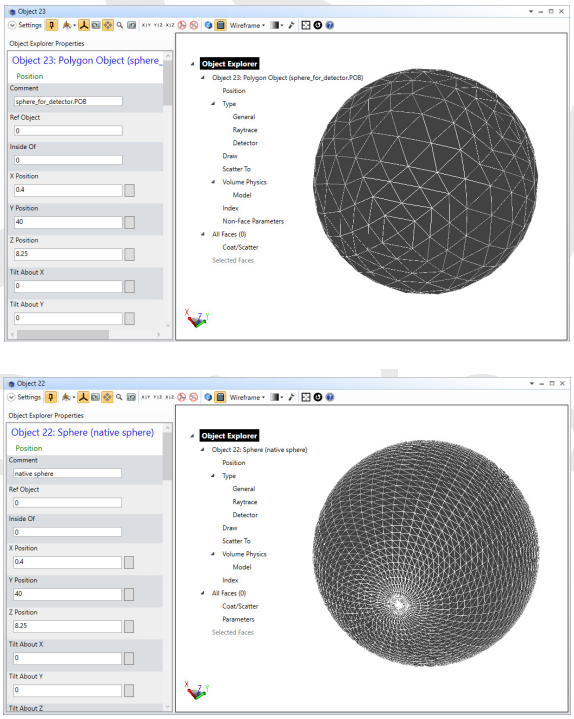

Fig. 12. A wireframe view in the "Object Editor" tool shows the difference in tessellation between a spherical polygon object on the top (with a user-selected number of facets) and a native sphere object on the bottom.

The resulting faceted structure can be easily seen by inspecting the polygon object with the “Object Editor” tool. Figure 12 shows the spherical polygon object on the left, and for comparison purposes the tessellated version of a native sphere object on the right (with varying surface triangle sizes and shapes as determined internally by OpticStudio). It should be clear that the polygon object version is much better suited for use as a detector.

The spherical polygon *.POB file is then inserted into the model as a “Polygon Object” and designated to be a detector object (see Fig. 13).

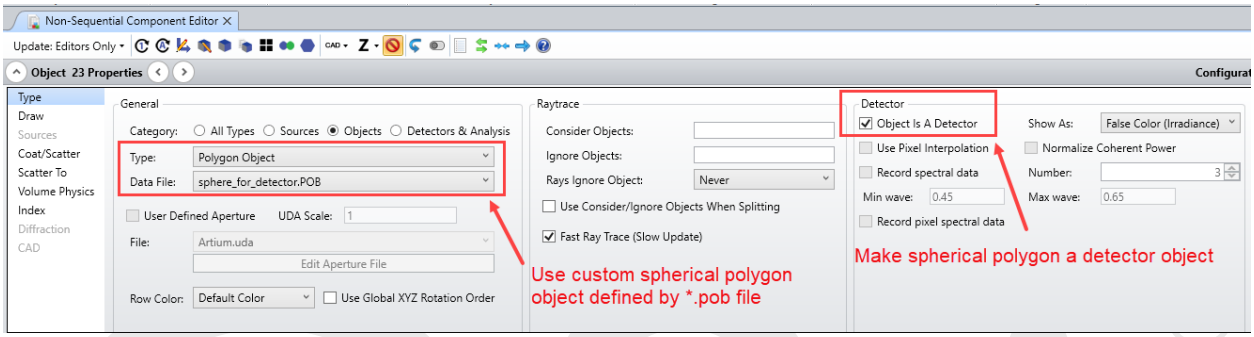

Fig. 13. After inserting the spherical polygon object into the model, turn it into a detector.

We prefer to detect only those rays that are externally incident on the polygon surface. However, polygon object detectors do not provide one-sided detection (only a Detector Rectangle allows that option). So, the next best solution is to make the polygon detector a fully absorbing volume. For our application this is a very reasonable approach given that a mask is highly absorbing anyway. So, in the NSE, we scale and position the spherical polygon detector to surround a single mask in the array, and also designate the detector object to be an absorbing volume (see Fig. 14).

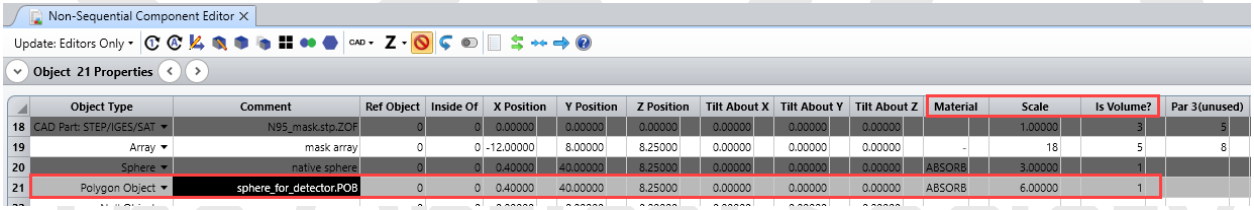

	Object Type	Comment	Ref Object	Inside Of	X Position	Y Position	Z Position	Tilt About X	Tilt About Y	Tilt About Z	Material	Scale	Is Volume?	Par 3(unused)
18	CAD Part: STEP/IGES/SAT	N95_mask.stp.ZOF	0	0	0.00000	0.00000	0.00000	0.00000	0.00000	0.00000		1.00000	3	5
19	Array	mask array	0	0	-12.00000	8.00000	8.25000	0.00000	0.00000	0.00000	-	18	5	8
20	Sphere	native sphere	0	0	0.40000	40.00000	8.25000	0.00000	0.00000	0.00000	ABSORB	3.00000	1	
21	Polygon Object	sphere_for_detector.POB	0	0	0.40000	40.00000	8.25000	0.00000	0.00000	0.00000	ABSORB	6.00000	1	

Fig. 14. The spherical polygon detector is scaled and set to be an absorbing volume.

Note that by placing the polygon detector <u>after</u> the mask array in the NSE listing, we can leverage OpticStudio’s object nesting rules be sure that the detector volume replaces the mask that it surrounds. The result is shown in Fig. 15, where the central mask has been chosen.

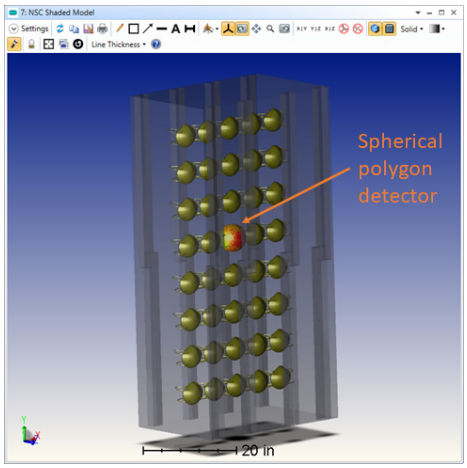

Fig. 15. Shaded model view showing a spherical polygon detector situated over a mask.

After running a ray trace, the polygon detector can display a color-coded version of the local irradiance on the pixels, for example, using false color as shown in Fig. 16.

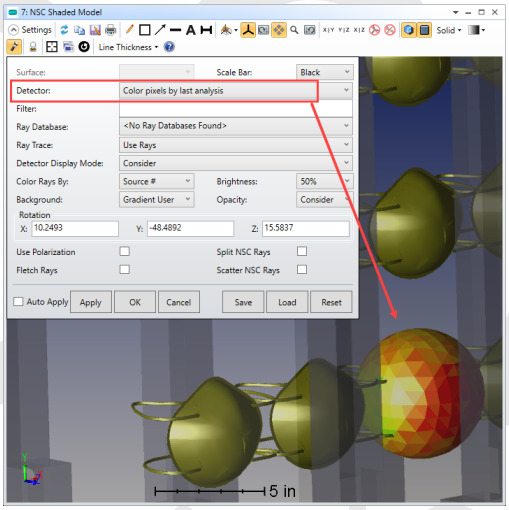

Fig. 16. Shaded model display with pixel irradiance values shown in false color.

A zoomed-in view of the detector is provided in Fig. 17 with the “Use Lighting” option turned off so as to provide a more accurate visual representation of the irradiance. It is seen that the weaker irradiance values (yellow and green pixels) are on pixels adjacent to neighboring masks that cause some shading. The total number of ray hits on the detector, along with the raw detector data, are available from the text listing in a “Detector Viewer” window. The data values can be cut-and-paste into a third-party analysis package such as Matlab and used to create an irradiance histogram as shown in Fig. 17 (bottom).

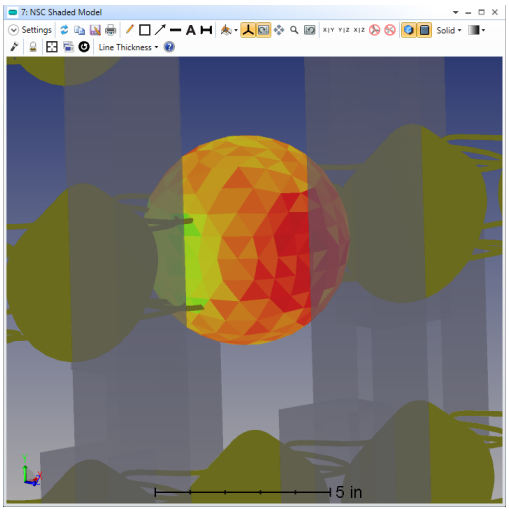

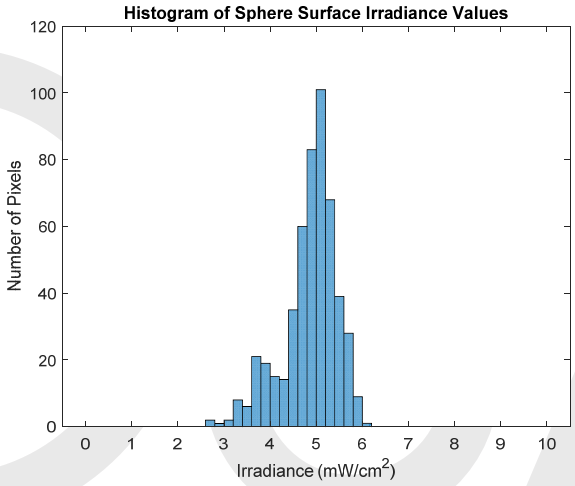

Fig. 17. Zoomed-in view of the spherical polygon detector showing the local irradiance variation over the detector surface. This mimics what the mask internal to the detector would "see." The pixel data are used to generate an irradiance histogram.

For this simulation run we used 10^6 rays/source, which produced over 15M total detector hits (or ~30K rays/pixel on average, corresponding to a ray-sampling SNR of sqrt(30K) = 173 which is very good, meaning negligible random ray noise artifacts and a corresponding high-fidelity result). From the histogram, we see the irradiance spans a range from 3-6 mW/cm^2. To ensure all portions of the mask surface receive at least 1 J/cm^2 exposure, we use the lower 3 mW/cm^2 value and conservatively estimate that an exposure time of (1 J/cm^2 ÷ 0.003 J/sec·cm^2) = 333 seconds = 5.5 minutes should be adequate for full decontamination.

3.2 Cylindrical Trash Can Geometry (3-4 masks)

A more compact geometry that can provide higher average irradiance, but accommodates fewer masks at a time, is based on a small cylindrical trash can. As shown in Fig. 4, there are eight lamps (6.9 watts each) mounted in a circular pattern around the interior sidewall of the can. The can has a slightly larger diameter at the top (20.5") compared to the bottom (18"), so the sidewall has a mild taper of about 2.75

degrees. Therefore, strictly speaking, the geometry is conical with a 5.5-degree full cone angle, but for practical purposes it can be considered quasi-cylindrical. The Source Tube in OpticStudio can be easily arrayed in a cylindrical format, but for this quasi-cylindrical geometry we insert each source as a separate object in the NSE. However, the lamp fixtures can by arrayed on a conical surface by using a parent object in combination with the "Array Ring" object having parameter values displayed in Fig. 18.

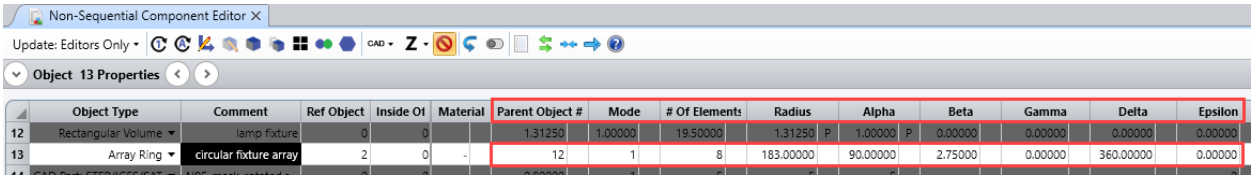

	Object Type	Comment	Ref Object	Inside Of	Material	Parent Object #	Mode	# Of Elements	Radius	Alpha	Beta	Gamma	Delta	Epsilon
12	Rectangular Volume	lamp fixture	0	0		1.31250	1.00000	19.50000	1.31250 P	1.00000 P	0.00000	0.00000	0.00000	0.00000
13	Array Ring	circular fixture array	2	0	-	12	1	8	183.00000	90.00000	2.75000	0.00000	360.00000	0.00000

Fig. 18. Lamp fixture array created by using the "Array Ring" object.

The fixtures are arranged on a slightly tapered conical surface (approximately cylindrical) by selecting the Mode = 1 option and rotating the array elements by 2.75 degrees about a y-axis located at z = 183" in the array's local coordinate system (i.e., the "Radius" parameter). This rotation point is approximately the vertex location of the cone, but adjusted somewhat to properly position the lamp fixtures against the interior wall of the can.

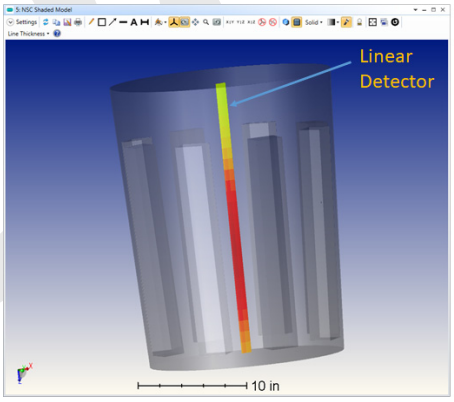

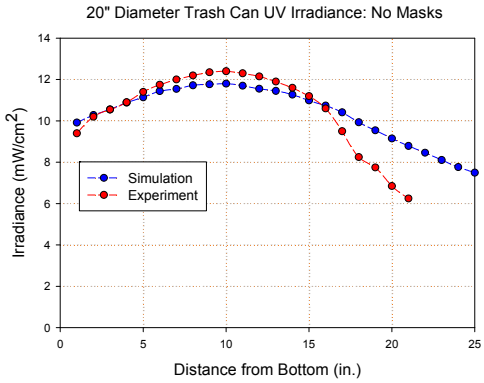

Fig. 19. Trash can geometry (no masks) with irradiance measured along the central axis.

Figure 19 depicts the resulting layout without masks installed. A thin, long Detector Rectangle is placed along the central axis. It is fully transparent, but set for single-sided detection in order to compare the results against experimental measurement. The results are plotted on the bottom panel of Fig. 19.

The correspondence between the simulation and experiment is reasonably good, particularly given the assumptions made in the model for various surface reflectivity/scattering properties. In the region surrounded by the lamps, the irradiance (without masks installed) varies between 10-12 mW/cm^2.

Of course, the more germane case is the one that includes the masks. For this model we place a linear array of three masks in the center. We also add a simple mask supporting frame fabricated from 1" PVC pipes (implemented as "Cylinder 2 Volumes") and combined together as a single "Boolean Native" object having aluminum foil surface properties (Table 1). We also modify the lamp fixtures to include 45-degree bevels along the two edges that parallel the lamp bulb, which better approximates the actual shape. This is done in OpticStudio by first creating the desired fixture cross-section as a user-defined aperture (UDA) file and then using it with an "Extruded" object. This extruded object now becomes the parent object for the Array Ring (see Fig. 18).

As with the cabinet design, we can again compute the local irradiance distribution over a mask surface by using an absorbing polygon object detector. For the more compact metal can arrangement, the choice of detector shape has a greater impact on the resulting perturbation to the ray trace, so simulation accuracy should be improved if the detector shape matches that of a mask (but the detector is made slightly larger so as to completely encompass the mask surface). We therefore opt for a *hemispherical* polygon detector. Again, the key is to create a volume with a polygon surface represented by triangles having approximately the same size that provide reasonably uniform surface sampling. Unfortunately, the "Create Polygon Object" tool cannot generate a hemisphere, so we devised a scheme to circumvent this limitation. We start with the spherical polygon described in the previous section. Then we construct a cylindrical volume that overlaps with half of the sphere and use a "Boolean CAD" object to subtract the overlap region,[1] thereby leaving just a hemisphere. However, the flat surface of this hemisphere has a very irregular native triangle representation that is ill-suited for pixelated detection. So, we employ an absorbing circular "Detector Surface" that is planar and is placed in contact with the flat surface of the Boolean CAD hemisphere. This circular detector has 32 annular zones (which matches the Boolean CAD Hemisphere) and 8 radial zones, and is comprised of a more regular set of triangular pixels. Construction of the resulting Polygon Hemisphere Detector is illustrated in Fig. 20.

[1] We use the Boolean CAD instead of the Boolean Native object because only the Boolean CAD version can be designated as a detector.

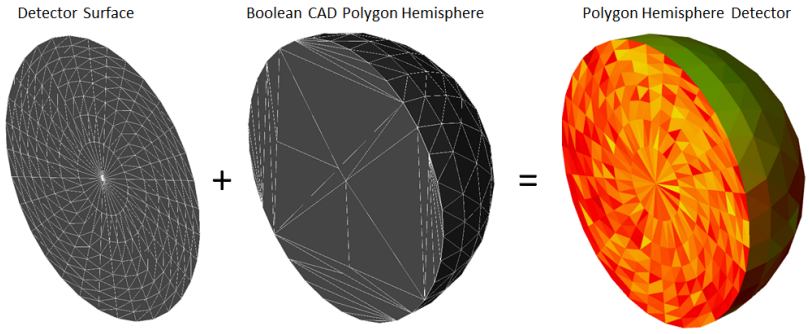

Fig. 20. Construction of a Polygon Hemisphere Detector as a composite of two separate absorbing detector structures. A circular Detector Surface (made with a strategic choice of annular and radial zones) is placed in contact with the flat surface on the Boolean CAD Hemisphere.

The radius of the circular detector surface is just slightly larger (by 0.005") than that of the Boolean CAD hemisphere to ensure that no rays hit any part of the Boolean CAD flat surface and generate spurious irradiance values for the associated irregular pixels. Also, in the NSE listing, it is important that the circular Detector Surface comes *after* the Boolean CAD hemisphere so that it takes precedence per OpticStudio's nesting rules. Putting all of these features together yields the final model illustrated in Fig. 21.

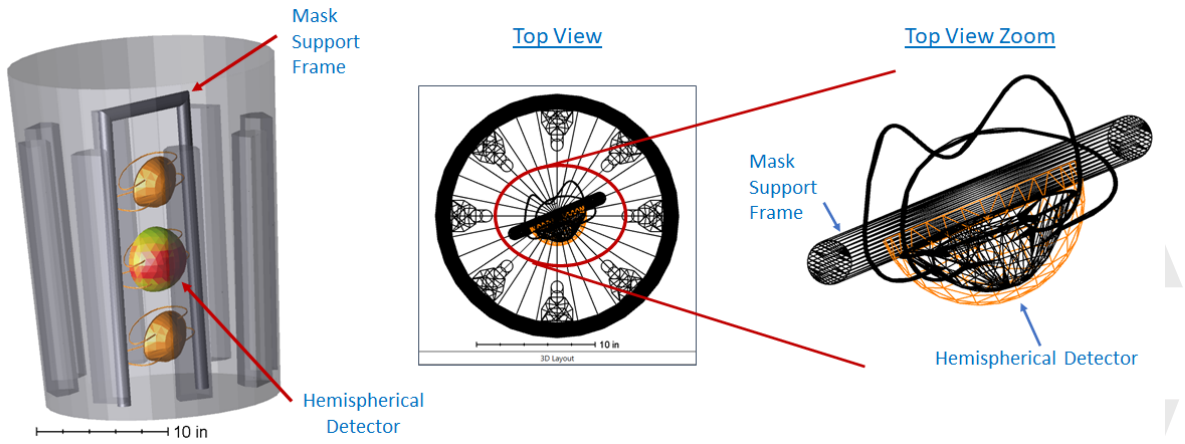

Fig. 21. Views of the quasi-cylindrical trash can model with masks and a support frame installed. The hemispherical detector of Fig. 20 is also included. The zoomed-in top view on the right shows the detector in relation to a wireframe version of a mask.

Lastly, the histogram on the right-side of Fig. 22 shows the local irradiance distribution over a mask, as measured by the composite hemispherical polygon detector (using 10^6 rays/lamp). In this case, text irradiance data are copied from the Detector Viewer window, for both the Detector Surface and the Boolean CAD hemisphere detector, and pasted into Matlab. The flat surface of the Boolean CAD hemisphere registers irradiance values of zero since this surface is covered by the circular Detector Surface. These zero values are discarded. The remaining irradiance values are appended to those from the Detector Surface, and the combined detector data set is used to create the histogram.

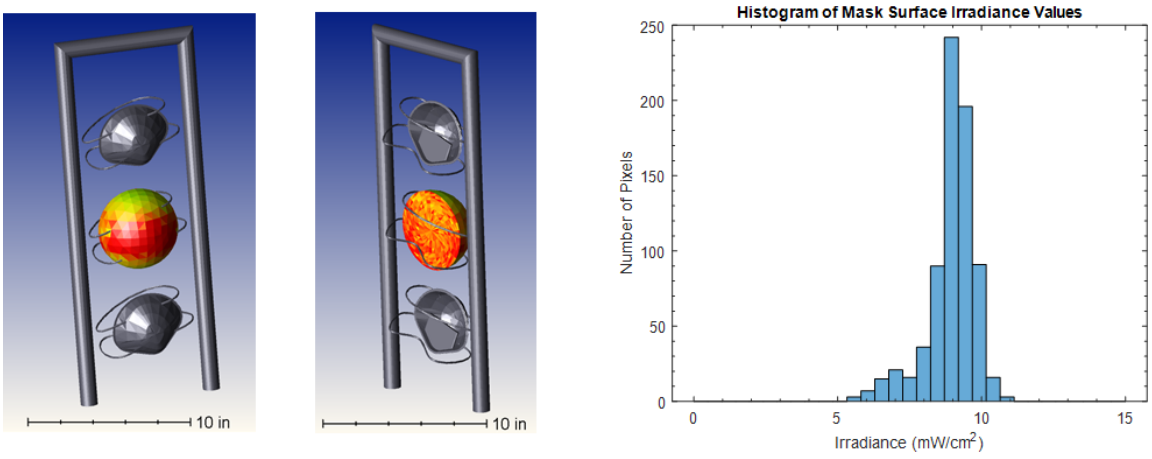

Fig. 22. Left: Two views of the composite hemispherical detector. Right: Histogram showing the corresponding pixel irradiance distribution.

The local irradiance values range from 6-11 mW/cm^2, which is about twice that for the cabinet geometry. Accordingly, the decontamination exposure time (based on the lower 6 mW/cm^2 value) is approximately half, or 2.25 minutes.

4. Summary

We have demonstrated the use of Zemax OpticStudio for modeling two different UV-C decontamination chamber geometries, namely a rectangular cabinet and a cylindrical can. All of the critical details related to model construction and data analysis have been highlighted and discussed. Our simulation results compare quite favorably to experimental measurements made without masks installed. This gives us confidence that the model can be extended to include mask arrays and yield accurate results. In particular, we leverage the use of spherical and hemispherical polygon detectors to estimate the local irradiance variations over a mask surface in the different geometries. From these results we can then recommend illumination times to reach the full decontamination exposure level of 1 J/cm^2.

Funding

This research was funded by the authors.

Acknowledgement

Zemax OpticStudio is a registered trademark of Zemax, LLC.

Disclosures

The authors declare no conflicts of interest.

References

1. Ultraviolet germicidal irradiation (https://en.wikipedia.org/wiki/Ultraviolet_germicidal_irradiation)

2. Technical Report for UV-C-Based N95 Reuse Risk Management, N95DECON consortium (https://www.n95decon.org/)

3. CDC, Decontamination and Reuse of Filtering Facepiece Respirators, (https://www.cdc.gov/coronavirus/2019-ncov/hcp/ppe-strategy/decontamination-reuse-respirators.html)

4. LADRepCo, Horsham, PA (https://www.labrepco.com/2020/04/07/a-solution-to-safely-reuse-n95-respirator-masks-shortwave-uvc-light-decontamination/)

5. Atomic Blue Group, Houston, TX (https://atomicbluegroup.com/)

6. M Health Fairview (https://www.mhealth.org/blog/2020/april-2020/m-health-fairview-rolls-out-new-uv-decontamination-process-for-n95-masks)

7. Nebraska Medicine (https://www.nebraskamed.com/sites/default/files/documents/covid-19/n-95-decon-process.pdf)

8. Martin Purschke, Mazzin Elsamaloty, Jeffrey P. Wilde, Nichole Starr, R. Rox Anderson, William A. Farinelli, Fernanda H. Sakamoto, Maryann Tung, Joshua Tam, Lambertus Hesselink, and Thomas M. Baer, "Construction and validation of UV-C decontamination cabinets for filtering facepiece respirators," *Appl. Opt.* (to be published)

9. Atlantic Ultraviolet Corporation®, Hauppauge, NY (https://www.buyultraviolet.com/biolux-uv-air-and-surface-irradiating-strip-fixtures)